Materials Science and Engineering A 508 (2009) 1–14

Contents lists available at ScienceDirect

Materials Science and Engineering A

journal homepage: www.elsevier.com/locate/msea

Review

Effect of 475 °C embrittlement on the mechanical properties of duplex stainless steel

J.K. Sahu [a,b,*], U. Krupp [c], R.N. Ghosh [a], H.-J. Christ [b]

[a] National Metallurgical Laboratory, Jamshedpur 831007, India
[b] Institut für Werkstofftechnik, Universität Siegen, 57068 Siegen, Germany
[c] Faculty of Engineering and Computer Sciences, FH Osnabrück, University of Applied Sciences, 49009 Osnabrück, Germany

ARTICLE INFO

Article history:
Received 23 June 2008
Received in revised form
30 November 2008
Accepted 6 January 2009

Keywords:
Duplex stainless steel
Ferritic phase
475 °C embrittlement
Tensile behaviour
Impact energy
Fracture toughness
Fatigue behaviour

ABSTRACT

The binary iron–chromium alloy embrittles in the temperature range of 280–500 °C limiting its applications to temperatures below 280 °C. The embrittlement is caused by the decomposition of the alloy to chromium-rich phase, α′ and iron-rich phase, α. This phenomenon is termed 475 °C embrittlement as the rate of embrittlement is highest at 475 °C. Primarily the investigations on 475 °C embrittlement were confined to binary iron–chromium alloys and ferritic stainless steels. Duplex stainless steel grades contain varying proportions of ferrite and austenite in the microstructure and the ferritic phase is highly alloyed. Moreover, this grade of steel has several variants depending on the alloy composition and processing route. This modifies the precipitation behaviour and the resulting change in mechanical properties in duplex stainless steels when embrittled at 475 °C as compared to binary iron chromium systems. The precipitation behaviour of duplex stainless steel at 475 °C and the effect on tensile, fracture and fatigue behaviour are reviewed in this article.

Contents

1. Introduction

Duplex stainless steel (DSS) is finding increased applications as structural material in critical components of nuclear power plants [1–4], chemical industries [5,6], oil and gas sectors [7,8], paper and pulp industries [9,10], transportation [11] and other general engineering applications because of higher strength, superior

* Corresponding author at: National Metallurgical Laboratory, Jamshedpur 831007, India. Tel.: +91 657 2345194; fax: +91 657 2345213.
E-mail address: jksahu@nmlindia.org (J.K. Sahu).

0921-5093/$ – see front matter © 2009 Published by Elsevier B.V.
doi:10.1016/j.msea.2009.01.039

resistance to stress corrosion cracking and better weldability [12]. The excellent combination of mechanical properties and corrosion resistance of duplex stainless steel is obtained from balanced amount of ferrite and austenite in the microstructure. However, this grade of steel embrittles when exposed in the temperature range of 280–500 °C limiting its application to temperatures below 280 °C. This phenomenon is termed 475 °C embrittlement as the rate of embrittlement is highest at 475 °C [13–15]. The embrittlement changes the tensile [16–22], fracture [23–32] and fatigue [33–47,23,48,49] behaviour of this steel.

The problem of the high temperature application of ferritic stainless steel as a result of 475 °C embrittlement was well known [13–15,50–52]. The decomposition of the ferritic phase to chromium-rich phase, α′ and iron-rich phase, α in the temperature range of 280–500 °C due to the presence of miscibility gap in iron–chromium binary alloy system embrittles the microstructure. Since this problem was inherent to ferritic microstructure research emphasis on the embrittlement problem in this temperature range was mostly confined to solely binary iron–chromium alloys and in some cases commercial grades of ferritic stainless steels [13–15,52].

DSS on the other hand contains both ferrite and austenite in varying proportions in the microstructure and is undergoing continuous evolution to newer grades primarily based on adjusting the chemical composition and processing route. Recent development of DSS occurs mainly in the area of alloying molybdenum, copper, nitrogen, etc. for further improving mechanical and corrosion properties. As a result, this grade has a wide range of compositional variation. Cast DSS grades such as CF3, CF8, CF8M, predominantly used in nuclear power industries have ferrite volume fraction in the range of 9–15%, where as the ferrite volume fraction of wrought DSS such as SAF 2205, used in chemical tankers, line pipes is as high as 50%. The chemical compositions of some cast and wrought grades of DSS are listed in Table 1 (these compositions are approximate only and is intended for a comparison of cast and wrought DSS). The 475 °C embrittlement limits the volume fraction of ferrite in the cast grades of DSS (CF3, CF8, CF8M) to below 15% in the microstructure [53]. The volume fraction of ferrite in the wrought grades however varies from as low as 25% to as high as 75%.

As only the ferritic phase is embrittled during aging treatment at 475 °C the degradation in mechanical properties directly depends on the state of the ferritic phase. The volume fraction, distribution in the matrix, grain size and grain shape of the ferritic phase are observed to affect the nature of precipitation and the degree of embrittlement [54]. The bcc–fcc structural difference gives rise to factors such as load sharing between the two phases due to a difference in elastic and plastic response [55,56], difference in the ability to resist crack propagation. The majority of work, on the effect of 475 °C embrittlement on mechanical properties is reported from nuclear power industries. Now-a-days even wrought DSS with a high ferrite content are subjected to this range of temperature and a limited number of studies on 475 °C embrittlement on wrought DSS are reported.

In the present paper, effort has been made to discuss in detail and assimilate the work done by different research groups on the mechanisms, kinetics and thermodynamics of α′ precipitation, changes in impact, tensile and fatigue behaviour of DSS as a result of 475 °C embrittlement. The work relating the precipitation characteristics to mechanical properties are discussed. The paper also suggests some of the gray areas where further investigations need to be carried out.

2. The 475 °C embrittlement

Reidrich and Loib [50] were the first to report embrittlement, caused by elevated temperature exposure of iron–chromium alloy system. They conducted bend test and observed that steels containing 19–23 at.% chromium showed poor ductility after 1000 h exposure at 500 °C. However, the ductility was not impaired when the samples were aged at 550 °C. This observation indicated that the embrittlement is sensitive to temperature in a very narrow range. Fisher et al. [57] were the first to suggest the decomposition of the ferritic phase in a binary iron–chromium alloy to chromium-rich phase (α′) and an iron-rich phase (α), in the temperature range of 280–500 °C. They observed fine spherical precipitates of diameter, 200 Å in steel samples containing 28.5 at.% chromium aged at 475 °C for 1–3 years. The precipitate observed by them had bcc structure containing about 80 at.% chromium and was nonmagnetic in nature. The lattice parameter of these precipitates was reported to be between that of iron and chromium. After the detection of precipitates caused by aging treatment and the resulting embrittlement, the focus of research shifted to identify the phases in iron–chromium binary alloy system in the temperature range of 280–500 °C that cause the embrittlement. William [58] was the first to propose explicitly, the existence of a miscibility gap in the iron–chromium phase diagram in the temperature range of 280–500 °C as the cause of precipitation of α′ as shown in Fig. 1. According to this phase diagram 475 °C embrittlement may be expected at temperatures below 516 °C in the composition range of 12–92 at.% chromium in iron–chromium binary alloy system. So this study was a confirmation of the earlier study by Reidrich and Loib [50] on the redissolution of α′ precipitate when aged at 550 °C. Blackburn and Nutting [51] completely redissolved the α′ after 24 h of aging at 550 °C. The neutron diffraction studies conducted by Vintaikin and Loshmanov [59] confirmed the clustering and decomposition of ferritic phase in the temperature range of 280–500 °C.

Some of the critical reviews on the theory of decomposition in metastable ferritic alloys were done by Cahn [60] and Hilliard [61]. These reviews discussed the thermodynamical distinction within the miscibility gap for: (a) spinodal decomposition; (b) nucleation and growth of α′. Spinodal decomposition refers to a reaction where two phases of the same crystal lattice type, but different compositions and properties, form due to the existence of a miscibility gap in the alloy system by means of uphill diffusion without nucleation. Thermodynamically this is possible at concentration between the points where the second derivative of free energy with composition equals zero. This phase separation process occurs at a very fine

Table 1
Chemical composition of cast and wrought grades of DSS, wt.%*.

	Grades	C	Mn	P	S	Ni	Cr	Mo	N	Cu
Cast	CF3	0.030	0.60	0.003	0.002	8–12	17–21	<0.5	–	–
	CF8	0.057	0.62	0.003	0.002	8.23	19.94	0.21	–	–
	CF8M	0.074	1.21	0.032	1.140	9.59	18.67	2.73	–	–
Wrought	2205	0.030	2.00	0.030	0.020	4.5–6.5	22–23	3.0–3.5	0.15	–
	2507	0.030	1.20	0.035	0.020	6.0–8.0	24–26	3.0–5.0	0.24	0.5
	255	0.040	1.50	0.040	0.030	4.5–6.5	24–27	2.9–3.9	0.25	2.0

* These comparisons are approximate only and are intended for a comparison of cast and wrought DSS.

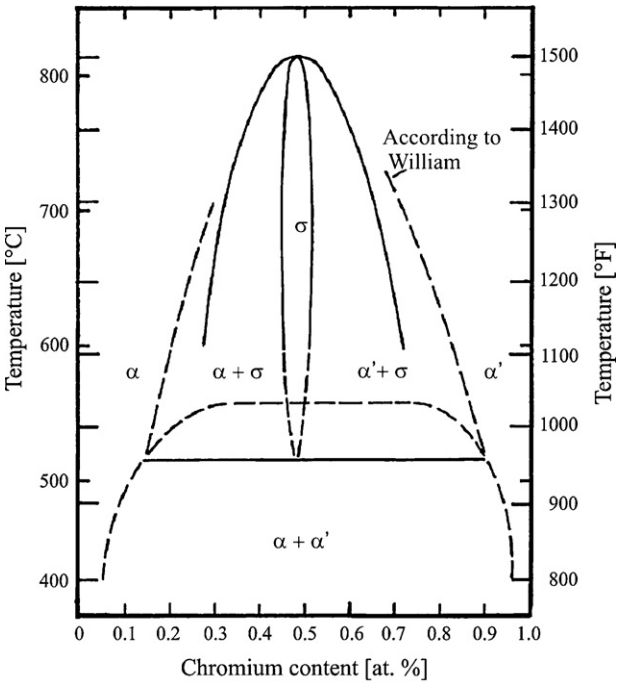

Fig. 1. Phase diagram of the iron–chromium binary system. Reprinted with kind permission from Springer from [58].

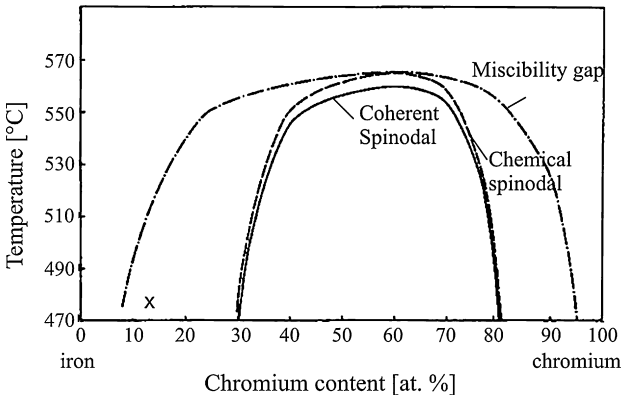

Fig. 2. Miscibility gap as proposed by William, calculated chemical spinodal, calculated coherent spinodal, x, indicate solubility limit of chromium in iron at 475 °C. Reprinted with kind permission from Springer from [14].

scale (of the order of only a few nanometers) and the presence of the α′ phase can only be detected through an atom probe field ion microscope [15]. According to Cahn [60] there should be no change in molar volume with composition in an infinite isotropic solid free from imperfections in order to have spinodal decomposition. So the sustainability of spinodal decomposition is very stringent for a multi component ferritic phase as in DSS, where many alloying elements other than chromium are partitioned to the ferritic phase. Chandra and Schwartz [14] tried to calculate the solubility of chromium in iron in the temperature range of 280–500 °C and predicted the boundaries within the miscibility gap for spinodal decomposition, nucleation and growth. Fig. 2 shows the miscibility gap as proposed by William [58] and the calculated chemical spinodal by the dashed line. The coherent spinodal line in the diagram is the corrected chemical spinodal taking into account the elastic strain energy due to 0.6% difference in the atomic size of iron and chromium. They studied the Mössbauer effect of 475 °C embrittlement of a series of iron–chromium binary alloys by varying the chromium content and estimated the solubility of chromium in iron to be 12 at.% at 475 °C. They predicted that only alloys with chromium content in excess of 12 at.% exhibit 475 °C embrittlement. Another important observation was that alloys with chromium content 12–30 at.% decomposed via a nucleation and growth mechanism.

Studying DSS via Mössbauer spectroscopy is always difficult as γ-austenite is paramagnetic and obscures the detection of paramagnetic α′ phase. However, Solomon and Levinson [13] successfully studied the effects of other alloying elements on 475 °C embrittlement with the help of Mössbauer spectroscopy and transmission electron microscopy in DSS and seven single-phase ferritic alloys. They showed that nickel promoted the formation of α′ whereas manganese, silicon and molybdenum did not influence the formation of α′. Miller and Russell [23] also have reported similar results.

Sahu [56] investigated a wrought grade of DSS, DIN W Nr. 1.4462 and observed needle-shaped precipitate after aging treatment at 475 °C for 100 h in the ferritic grains as shown in Fig. 3a. He identified these precipitates as needles of α′. He also observed stacking of these needles into arrays as shown in Fig. 3b.

Weng et al. [48] carried out detailed investigations on the nano-scaled structure of the low-temperature aged specimens of a 2205 wrought alloy with the help of field-emission gun transmission electron microscopy. They noticed the ferritic phase giving a modulated contrast after aging and there is a sudden change to an even contrast in austenitic phase, when observed under TEM. This mottled image with the gradient in contrast, which has the appearance of an orange-peel is shown in Fig. 4. The modulated microstructure

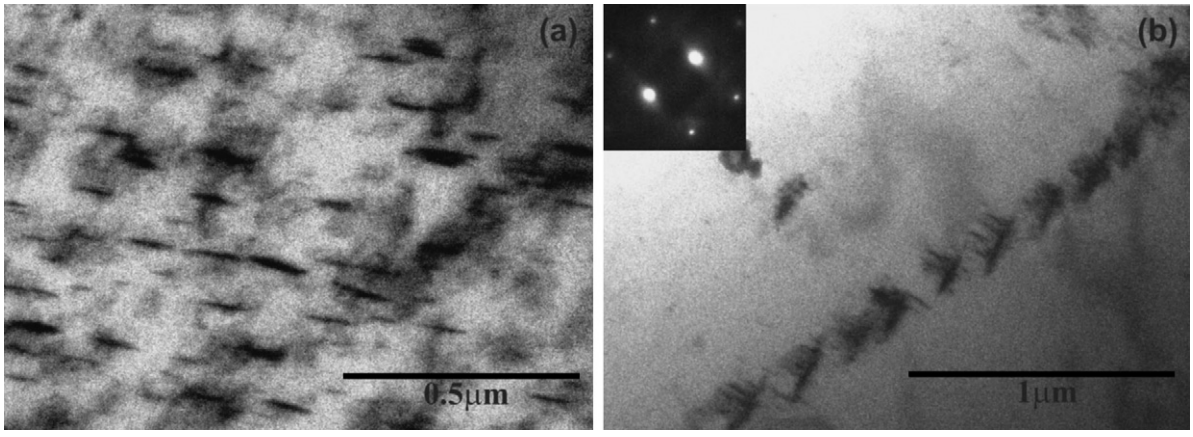

Fig. 3. (a) Needle like precipitates observed in the ferritic phase of DSS grade DIN W Nr. 1.4462 after aging treatment at 475 °C for 100 h; (b) same grain observed in g = (0 $\bar{1}$ $\bar{1}$) diffraction condition [56].

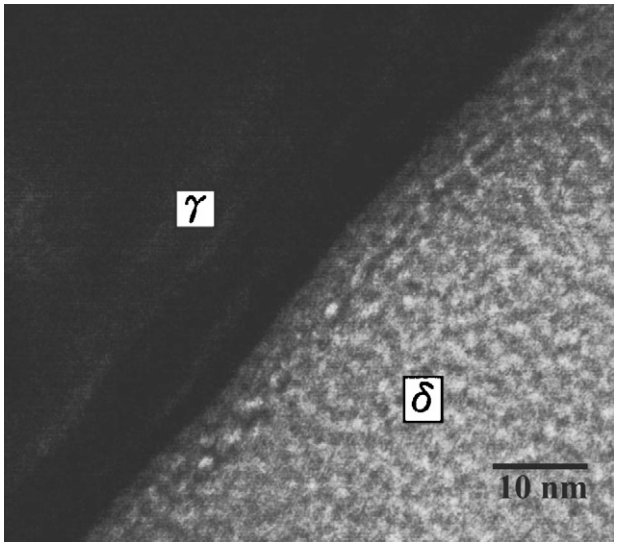

Fig. 4. Modulated contrast observed in the ferritic phase of DSS grade 2205 aged at 475 °C for 2 h. Reprinted with kind permission from Elsevier from [48].

coarsens with the time of aging, maintaining the similar morphology. This group has further studied the extent of phase separation that takes place due to 475 °C embrittlement using a FEG-TEM containing an EDS. The fine scale isotropic spinodal decomposition of ferritic phase revealed chromium-rich bright image domains and iron-rich dark image domains, i.e. α and α′ phases, separately. It also revealed that molybdenum and manganese were partitioning to the α′ phase, while nickel was partitioning to the α phase.

The three-dimensional α′ phase had been reconstructed by Miller and Bentley [62] and they suggested that the α′ phase forms a typical complex interconnected network structure from the studies conducted by atom probe field ion microscope. Similar atom probe field ion microscopy studies on CF series of cast alloys also had been performed [1,20], and the morphology, size distribution and chemical concentration profile of the α′ precipitates have been determined. The studies on the cast alloys revealed that the phase boundary carbides played a significant role in thermal embrittlement at temperatures greater than 400 °C, but has insignificant effect on the embrittlement at exposure temperatures less than 400 °C [52].

Mateo et al. [63] studied the G-phase precipitation in detail in an AISI 329 grade of DSS and observed an incubation time from the completion of spinodal decomposition to the nucleation of G-phase. After 200 h aging treatment at 475 °C, they observed very fine spots in TEM bright field image. The uniform G-phase particles in the grain body were observed only after 15,000 h of aging at 475 °C. This indicates that the possibility of G-phase precipitation in the ferritic phase requires long duration aging treatment at 475 °C. The carbide and nitride precipitates are mostly observed in grain boundaries [53,54].

Recently Bliznuk et al. [64] studied the effect of nitrogen on short-range atomic order in the ferritic phase of a duplex steel and observed that with increasing content of nitrogen in steel, its concentration in ferrite increases. They obtained that an increase in the nitrogen content from 0.17 mass% in steel SAF2205 to 0.25 mass% in steel SAF2507 led to short-range atomic ordering of chromium and molybdenum atoms, whereas further increase of the nitrogen content (0.62 mass%) was accompanied by their clustering. The opposite behaviour is obtained for the distribution of nickel atoms. However, nitrogen-caused change in the distribution of chromium, molybdenum and nickel atoms in ferrite could not prevent the 475 °C brittleness caused by the decomposition of the ferritic phase.

So the different possibilities for the segregation or precipitation in the ferritic phase resulting from the aging treatment at 475 °C reported so far are:

1. Formation of α′ either through spinodal decomposition (infinitesimal composition fluctuation in a solid solution) or through the mechanism of nucleation and growth.
2. Formation of G-phase.
3. Precipitation of carbides and nitrides at grain boundaries.

The kinetics of 475 °C embrittlement have been determined through indirect observations such as changes in certain mechanical properties like hardness [23], impact energy [56] or saturation of certain microscopic features [48]. The kinetics of precipitation plays a very important role for some of the critical engineering components particularly in nuclear power plants. So majority of investigations on kinetics of 475 °C embrittlement in DSS are reported from laboratories working on the materials used in nuclear power plants [24–26]. These investigations are mostly reported on CF3, CF8 and CF8M cast grades of DSS.

Sahu [56] observed that the deterioration of impact energy for DSS grade DIN W Nr. 1.4462 fit into a sigmoidal shape when plotted on a semi-log scale with time of aging at 475 °C as shown in Fig. 5. He obtained a value of 8 J for 100, 200 and 300 h of aging treatment and concluded that the embrittlement reaches saturation in 100 h for the investigated grade.

Miller and Russell [23] made comparison of the rate of decomposition of the ferrite in iron–45 wt.% chromium, iron–45 wt.% chromium–5 wt.% nickel alloys and two CF3 grades of DSS during long-term aging at 400 °C. According to this group the addition of nickel to the binary iron–chromium alloy accelerated the kinetics of decomposition and significantly increased the hardness of the alloy as shown in Fig. 6. Although the hardness data from the ternary alloys are similar to those of the ferritic phase in the DSS, they observed significant differences in the scale and composition amplitudes of the α and α′ phases. They investigated the extent of phase separation by determining the difference in the composition amplitudes of the α and α′ phases as a function of aging time at 400 °C. It is evident that the kinetics of precipitation plays an important role in the deterioration of mechanical properties. As shown by Miller and Russell the composition also plays a key role in determining the kinetics of precipitation. When in one hand

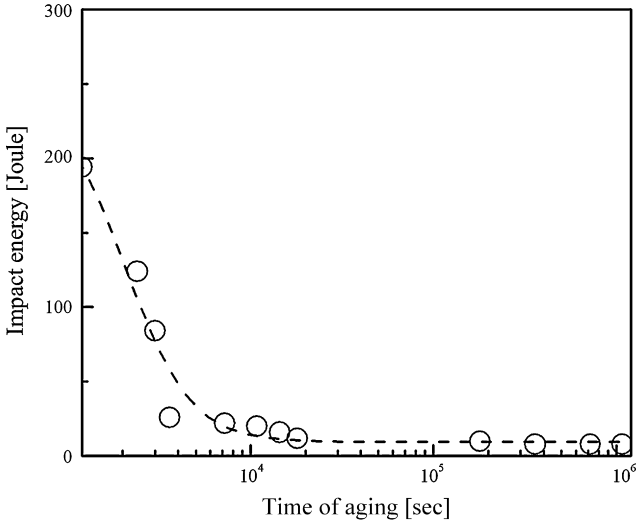

Fig. 5. Variation of impact energy with time of aging at 475 °C for DSS grade DIN W Nr. 1.4462 [56].

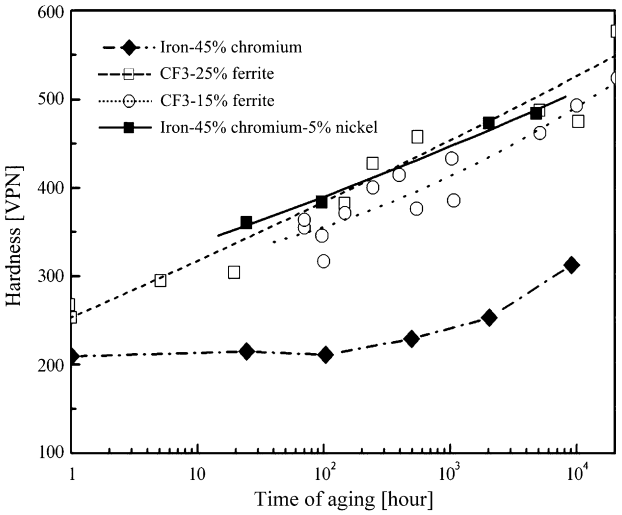

Fig. 6. Hardness of the iron–45% chromium–5% nickel alloy as a function of aging time at 400 °C. Comparable data from the iron–45% chromium binary alloy and the ferrite phase in two CF3 stainless steels for the same temperature are included for comparison. Reprinted with kind permission from Elsevier from [23].

there is a constant effort to improve the mechanical properties by alloying DSS further with copper, nitrogen, etc., effect of these alloying elements on α′ precipitation is a subject of extensive further research.

Grobner [15] reported that in the temperature range of 371–482 °C iron–chromium alloy with 18 at.% chromium embrittled in times as short as 2 h, where as with 14 at.% chromium embrittlement was observed after longer exposure time. This is a clear indication of the sensitivity of this embrittlement to alloy composition. According to Grobner interstitial element accelerated the embrittlement caused by precipitation of α′ phase on dislocation whereas substitutional alloying elements such as molybdenum and titanium did not substantially affect the kinetics of embrittlement.

The distribution of ferritic phase in the matrix, their grain size and grain shape play a very important role in determining the degree of embrittlement. As only the ferritic phase is embrittled during aging at 475 °C, the degradation in material properties directly depends on the amount and morphology of the ferritic phase. It has been established that 475 °C embrittlement is a major concern only when the volume fraction of the ferrite exceeds approximately 15–20% [32]. When the ferrite content in the microstructure is less than or equal to 15%, it remains as isolated pools contained within the austenite. In this case, the overall toughness of the alloy is not significantly affected even if the ferritic phase is embrittled. However, when ferrite levels are greater than 15% in the microstructure a continuous path of embrittled phase is formed during aging affecting the toughness of the component considerably. However, some recent evidences in the nuclear power plant components shows that ferrite levels in the range of 10–15% in the CF8M cast stainless steel castings may also be subjected to significant thermal embrittlement [56]. The grain size tends to be large, and the ferrite spacing (average distance between ferrite islands) is increased in heavy-section castings. With increasing ferrite spacing at constant ferrite content, the size of the ferrite island increases and the probability of a continuous path of ferrite through the thickness of the cast component increases. Bonnet et al. [55] selectively dissolved the austenite phase from samples of CF8M and found that the ferrite phase remains continuous at ferrite volume fractions as low as 5% Therefore, the thermal ageing of Grade CF8M with such a ferrite distribution needs to be evaluated.

3. Effect of 475 °C embrittlement on mechanical properties

It is established that aging, in the temperature range of 280–500 °C, results in a significant deterioration of mechanical properties. The embrittlement affects tensile, fracture and fatigue behaviour. In this section the effect of 475 °C embrittlement on tensile, fracture and fatigue behaviour are reviewed in separate sections.

3.1. Tensile behaviour

Before discussing the results obtained on the effect on 475 °C embrittlement on tensile behaviour of DSS, it is important to note that the structural incompatibility between the ferritic and austenitic phase modify the tensile behaviour [16]. When it comes to tensile strength ferrite is usually stronger than austenite for the same interstitial content. However, the solubility of carbon or nitrogen in austenite is much higher compared to ferrite [17]. In DSS nitrogen gets preferentially partitioned in a way that austenite becomes stronger than ferrite [18]. It was reported that in super DSS grades the amount of nitrogen dissolved in austenite is as high as 0.45 wt.% when the average nitrogen content is 0.27 wt.% and despite higher strength due to preferential nitrogen partitioning more plastic deformation occurred in austenite compared to ferrite as compressive residual stress build up in the ferritic phase during cooling. Strength is also grain size dependent. The grain size in a DSS is usually smaller than that of ferritic and austenitic stainless steel of corresponding chemical composition. This is explained by mutual hindering of growth of the ferrite and austenite grains. If the effect of grain size and partitioning of interstitial is compensated then the strength of DSS is controlled by the stronger ferritic phase. Toughness of DSS is very high due to the presence of austenite in the matrix. Austenite retards the cleavage fracture of ferrite. However, toughness is reported to be very sensitive to the precipitation of secondary phases.

Zielinski et al. [19] studied the evolution of dislocation structure in a solution annealed DSS by in situ TEM straining experiment and reported that the evolution of dislocation structure during straining was dependent on the orientation relationship between the two phases. In the case of special orientation relationships, the slip markings in the ferrite, produced by the dislocations emitted from the boundary, indicate the compatibility of easy slip systems in the two phases, which favours a strong localization of strain. In the case of random orientation relationships, the incompatibility of the easy slip systems in austenite and ferrite results in the cross slip of the dislocations emitted from the boundary into the ferrite grains leading to multiplication and the formation of dislocation loops and debris. They attributed the high flow stress of DSS to the particular slip transfer mechanism related to the random orientation relationships between the austenite and ferrite. Bugat et al. [20] performed in situ tensile test on DSS aged at 400 °C for 700 h to characterize strain fields and monitor the sites of damage nucleation. According to them damage preferentially initiates in areas, where the common slip system of the bicrystal has a low Schmid factor.

Hilders et al. [21] studied the effect of 475 °C embrittlement on fractal behaviour and tensile properties of DSS and observed dimple type of fracture mode for small aging times and transgranular as well as dimple rupture for 24, 40, and 120 h of aging. They also observed decrease in fractal dimension and the true fracture strain with increase in time of aging.

Gironès et al. [22] studied the dynamic strain aging effects on super DSS at temperatures ranging from 275 to 475 °C. They reported that the activation energy for serrated flow, which is used as a parameter to identify the mechanism of dynamic strain aging, is too high for interstitial solutes and too low for substitutional ones

to migrate to mobile dislocations to pin them through bulk diffusion both in austenite and ferrite.

3.2. Fracture behaviour

The most significant effect of the 475 °C embrittlement is the sudden drop in impact toughness. Sahu [56] observed that the impact energy of DSS grade DIN W Nr. 1.4462 drops from 260 J in the annealed condition to 8 J after aging treatment at 475 °C for 100 h. He attributed the drop in impact energy value to the inability of the ferritic phase to form deformation twins in the aged condition through TEM examination. Devillers-Guerville et al. [24] showed that the micromechanism of impact fracture at room temperature of a cast grade of DSS containing about 20 wt.% ferrite, embrittled at 400 °C are: (i) nucleation of cleavage cracks grouped in millimetric clusters in the ferritic phase; (ii) growth of the cavities by the plastic deformation of austenitic phase; and (iii) coalescence of the cavities to form a macroscopic crack. They observed no strain rate effect on the embrittled material when tested at room temperature. Druce et al. [26] studied the effect of notch depth, notch acuity and side grooving on the impact fracture behaviour of a cast DSS containing 25 wt.% ferrite in the temperature range of −200 to +300 °C. They reported that increasing specimen constraint is found to have a marked influence on fracture mode, the temperature for the onset of low-to-high fracture energy transition, and the fracture energy per unit ligament area associated with fracture at elevated temperature. On the basis of these test data they came out with optimum specimen geometry for monitoring the effect of 475 °C embrittlement on toughness and determining embrittlement kinetics.

The embrittlement at 475 °C causes severe impairment of the fracture toughness of DSS [42–45]. For the wrought grades like 2205, which are used in areas, where fracture based design is not extensively used, work reported on the fracture evaluation of these grades of DSS is very scarce. However, cast DSS grades like CF3, CF8, CF8M, used in many parts in the reactor vessel internal (RVI) such as in the lower support casting or forging, flow-mixing device and in the primary piping section such as in the combustion engineering surge nozzle at the hot leg, in combustion engineering safety injection nozzle and the elbows of PWR in nuclear power plants, are designed based on fracture mechanics approach. The lowering of fracture toughness as a result of 475 °C embrittlement is a matter of grave concern for these grades of DSS. The operating temperature of a PWR typically falls between 280 and 300 °C and at this temperature aging takes place after prolong exposure. For this reason the fracture toughness of an embrittled material has never been a matter of concern for the design engineers at the time of initial installation of the component. However, after exposure for long years the embrittlement results in a drop of fracture toughness and estimation of residual fracture toughness of a service-exposed material has been a major concern for engineers. The fracture toughness for these components is either estimated by using some empirical relation or by some alternative experimental technique as normal laboratory techniques are extremely difficult for the service-exposed components.

Tujikura and Urata [27] evaluated the integrity of the primary coolant piping for an initial PWR plant in Japan by means of elastic plastic fracture mechanics (EPFM) analysis. They applied EPFM mathematics to evaluate fracture toughness, as fracture in DSS after thermal embrittlement is recognized to be ductile [32]. So it was appropriate to apply this concept for the evaluation of the stability of the assumed crack. For this study they had chosen the location to be the hot leg piping at the reactor vessel outlet nozzle since both the temperature and imposed load are more severe and ferrite content was relatively high in the evaluating plant. The evaluation results showed that the crack will not grow into an unstable fracture and the integrity of the piping will be secure, even when such through-wall crack length is assumed to be as large as the fatigue crack length grown for a service period of up to 60 years.

Table 2
The parts of primary circuit elbows and heat treatment conditions for fracture toughness study [28].

Products	Mark	Thermal aging treatment
90° Elbow	EL	3000 h at 400 °C
Plate	CC	1000 h at 400 °C
Plate	DI	10,000 h at 400 °C
50° Elbow	EK	30,000 h at 350 °C
Plate	DI	700 h at 400 °C
50° Elbow	EK	30,000 h at 325 °C

Jayet-Gendrot et al. [28] attempted fracture toughness assessment with mini-CT specimens taken from the skin of primary circuit elbows. They carried out the tests for six different parts (Ref. Table 2) of primary circuit elbows and compared the results obtained from a 0.4T-CT specimen to 1T-CT specimen. It can be seen from Fig. 7 that for all the materials, the (J, Δa) points obtained using mini-CT specimens are in good accordance with the points obtained using 1T-CT specimen. Scatter for both the geometries are of same order. They also compared the results with the fracture toughness values obtained from predictive formulae. After the validation, they showed that such mini-CT specimens were representative and have proposed guidelines for further practice.

Le Delliou et al. [29] had conducted bending tests in an elbow of the main primary circuit of a pressurized water reactor, which contained a semi-elliptical circumferential notch as well as casting defects located on the flanks and had shown that the notch did not initiate even at the maximum applied bending moment.

Mathew et al. [30] used automated ball indentation method to evaluate the degradation in mechanical and fracture properties as a result of low-temperature aging. They carried out tests after aging at 400 °C for 6, 12, 18 months and have reported that there was a progressive decrease in indentation energy to fracture.

Earlier estimation of residual fracture toughness was made using predictive formulae based on chemical composition and aging conditions. Chopra and Chung [31] had made a conservative estimation of fracture toughness and J–R curve of DSS after thermal aging from the estimated room temperature Charpy V-notch impact energy. This curve defined the resistance of thermally aged cast stainless steel material to ductile, stable crack growth. The J–R curve was expressed by the power law relation in Eq. (1).

$$J = C\dot{A}_a n \tag{1}$$

where J was determined according to ASTM Specifications E 813-85 and E 1152, $\dot{A}_a$ was the crack extension, C and n were constants. Correlations were developed between these constants and the estimated Charpy V-notch impact energy to determine the lower bound J–R curve at PWR operating temperatures. These correlations accounted for differences between statically and centrifugally cast materials. The degree of conservatism in this J–R curve is low if both the estimated room temperature and operating temperature Charpy V-notch impact energies are on the upper shelf (greater than about 80 J/cm^2), but the degree of conservatism is higher if the room temperature impact energy is on the lower shelf. These correlations and the calculated values of C_{Vsat} can be used to estimate lower bound fracture toughness after long-term thermal ageing.

Example estimates of the lower bound fracture toughness of Grade CF8 and Grade CF8M cast stainless steel that are within ASTM Specification A 351 and have a ferrite content greater than 15% are listed in Table 3. The corresponding values of C_{Vsat}, the constants C and n for the J–R curves at 290 °C, and the lower bound fracture toughness, J_{Ic} (J at crack extension of 0.2 mm), for both statically and centrifugally cast materials are also listed in Table 3 [32]. The lower bound fracture toughness of Grade CF8M is lower than that

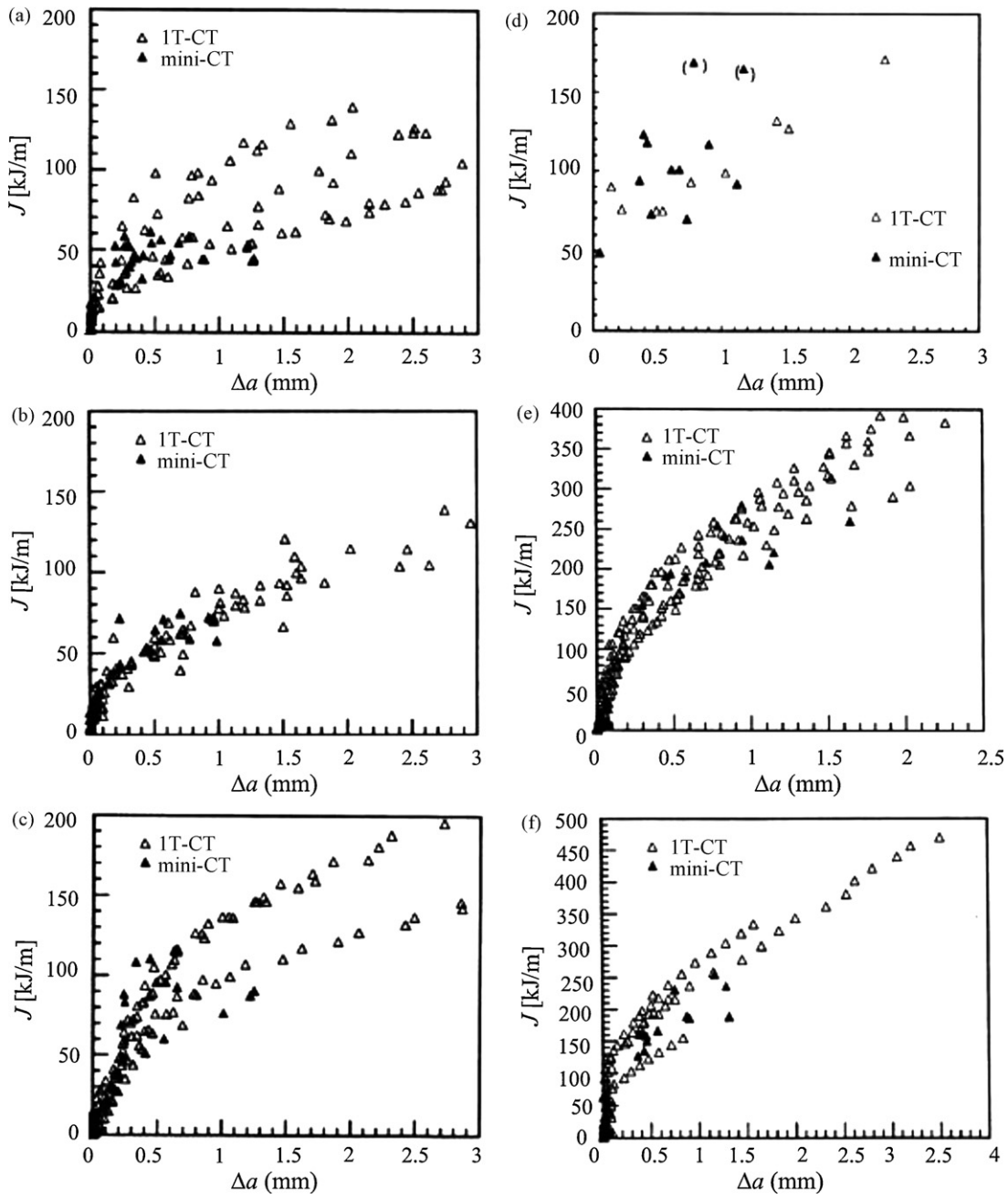

Fig. 7. J–Δa results at 320 °C for material: (a) EL aged 3000 h at 400 °C; (b) CC aged 1000 h at 400 °C; (c) DI aged 10,000 h at 400 °C; (d) EK aged 30,000 h at 350 °C (the crack deviated from side groove plane and the result was not taken into account); (e) DI aged 700 h at 400 °C; (f) EK aged 30,000 h at 325 °C. Reprinted with kind permission from Elsevier from [28].

of Grade CF8. In addition, the lower bound fracture toughness of statically cast material is lower than that of centrifugally cast material. These lower bound toughness values are for steels with ferrite content greater than 15%, which is higher than the typical average ferrite content in the nuclear industries.

In spite of the fact that safe values of residual fracture toughness can be predicted through empirical formulae based on chemical composition and aging conditions, efforts have been put to experimentally determine the fracture toughness values of the service-exposed material. Though standard fracture toughness

Table 3
Estimates of service temperature (290 °C) lower bound fracture toughness of cast grade DSS CF8 and CF8M, both statically cast and centrifugally cast with ferrite volume fraction greater than 15% [32].

Cast grade DSS	Saturation room temperature impact energy C_{Vsat} (J/cm^2)	Statically cast DSS			Centrifugally cast DSS		
		C	n	J_{Ic} (kJ/cm^2)	C	n	J_{Ic} (kJ/cm^2)
CF8	25	251	0.32	150	330	0.32	197
CF8M	20	167	0.30	103	195	0.30	120

tests are not possible due to severe operating conditions in the areas of PWR, non-standard tests are proposed to determine the fracture toughness values.

3.3. Fatigue behaviour

The factors those are known to influence the fatigue behaviour of DSS are:

1. Alloy composition [65–67].
2. Volume fraction of ferrite [32,42,53,54,61].
3. Processing route (cast and wrought) [61].
4. Texture [68].

Some of the above-mentioned factors also are known to have pronounced effect on the change in cyclic stress–strain behaviour and fatigue life of DSS due to aging treatment at 475 °C. So a discussion on the change in fatigue behaviour of DSS due to aging treatment at 475 °C must be done in conjunction with the above-mentioned factors. For example, Llanes et al. [36] observed ferrite like deformation mechanism and fatigue softening at $\Delta\varepsilon_{pl}/2 = 1.2 \times 10^{-3}$ for the AISI 329 grade of DSS in the aged condition (0.074 wt.% nitrogen, 38%γ62%α, wrought), while Vogt et al. [42] for their alloy BöA920 grade of DSS (0.4 wt.% nitrogen, 70%γ30%α, wrought) observed no change in fatigue resistance even at $\Delta\varepsilon_{pl}/2 = 5.3 \times 10^{-3}$ after aging treatment at 475 °C. This difference may be attributed to several factors such as nitrogen content, ferrite volume fraction.

DSS is undergoing continuous evolution to newer grades primarily based on adjusting the chemical composition. The most important is the increase in nitrogen content. Nitrogen affects the cyclic stress–strain behaviour and fatigue life of DSS [65–67]. It is austenite stabilizer and strengthens austenite by solid solution strengthening mechanism. A stronger austenitic phase results in strain partitioning to the ferritic phase. And the response of the ferritic phase to this strain partitioning will be different in plane-annealed and aged conditions. Moreover, recently nitrogen is also found to have establishing short-range order of chromium in δ-ferrite [63]. Some of the grades of DSS used for the study on fatigue behaviour are listed in Table 4 with the nitrogen content and references.

Table 4
Different commercial grades of DSS used for studying the fatigue behaviour.

Grades	Nitrogen content (wt.%)	Reference
AISI 329	0.0072	[36]
SAF 2205	0.15	[48]
DIN W Nr. 1.4462	0.17	[56,69]
SAF 2507	0.24	[70,71]
A905	0.35	
BöA920	0.4	[42]

Nitrogen addition is thought to be beneficial for the fatigue life of the material. However, Akdut [65] observed that contrary to single-phase austenitic stainless steels only increasing the nitrogen content in DSS did not increase fatigue life, but nitrogen in combination with the morphological scale and anisotropy apparently altered the cyclic stress strain curve. This means the beneficial effect of nitrogen on fatigue behaviour can be realized only with certain morphology. The conventional concept of microstructural barrier in single-phase materials sometime does not explain the low cycle fatigue behaviour adequately. Stolarz and Foct described that the physical properties and the degree of plastic deformation in the neighbouring grain or particle determine the resistance of a barrier [41]. Girones et al. [68] studied the influence of texture on the surface damage mechanisms developed in cyclically loaded aged DSS. The rolling or recrystallization texture is known to determine the local crystallographic orientation and this in turn influences the evolution and growth of surface damage [69,70]. Alvarez-Armas et al. [66] observed that the most important feature of the dislocation structure developed just beneath the surface of the fatigued specimen corresponds to the intense shear bands oriented in the direction of the shear plane crossing grains and phases when the *K–S* relationship is satisfied. This observation further strengthens the studies made by Girones et al. [68] on the indirect influence of texture on fatigue damage.

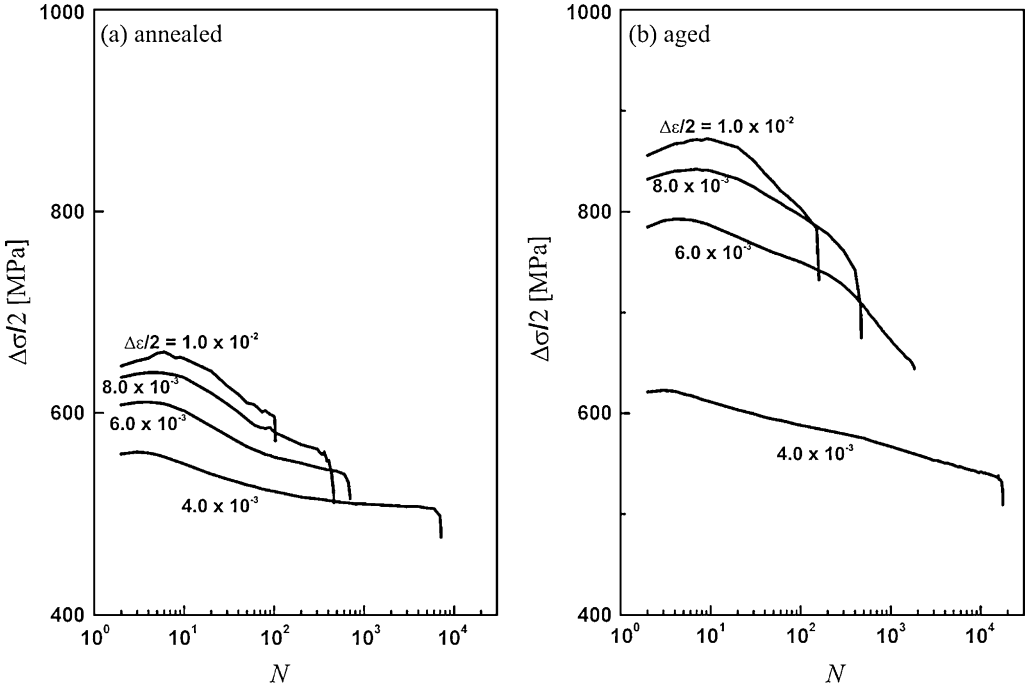

Fig. 8. Cyclic hardening/softening curves for DSS grade DIN W Nr. 1.4462 (a) annealed (b) aged (475 °C for 100 h) condition [56].

3.3.1. Cyclic hardening softening behaviour

Sahu [56] conducted total strain controlled fatigue test at $\Delta\varepsilon/2$ values 4.0×10^{-3}, 6.0×10^{-3}, 8.0×10^{-3} and 1.0×10^{-2} for DSS grade DIN W Nr. 1.4462 in annealed and embrittled (aged at 475 °C for 100 h) condition and observed that the deformation curves in the annealed condition have three discernible stages: (i) cyclic hardening, (ii) cyclic softening, and (iii) cyclic saturation. In the aged condition he observed two discernible stages: (i) cyclic hardening and (ii) cyclic softening till final failure for all values of strain amplitudes. The life span of each of the above stages was observed to be a function of strain amplitude both in annealed and aged condition, e.g. (i) he observed a prolonged cyclic saturation at $\Delta\varepsilon/2 = 4.0\times10^{-3}$ and the period of cyclic saturation decreased with increase in strain amplitude in the annealed condition, (ii) cyclic softening was gradual at $\Delta\varepsilon/2 = 4.0\times10^{-3}$, 6.0×10^{-3} and 8.0×10^{-3}, whereas rapid softening was observed for $\Delta\varepsilon/2 = 1.0\times10^{-2}$, and (iii) cyclic softening was rapid with increase in the value of strain amplitude in the aged condition as shown in Fig. 8.

Alvarez-Armas et al. [70] conducted total strain controlled fatigue testing ($\Delta\varepsilon/2 = 3.5\times10^{-3}$, 4.0×10^{-3}, 5.0×10^{-3}, 8.5×10^{-3}, 9.5×10^{-3}) of SAF 2507 grade of super DSS containing 0.236 wt.% nitrogen. They categorized the cyclic hardening softening response observed by them into three well-defined plastic strain ranges shown in Fig. 9a. Plastic strain ranges between 7.5×10^{-4} and 2.5×10^{-3} are identified by a long softening followed by a long saturation stage, while between 4.0×10^{-3} and 6.0×10^{-3}, a small initial cyclic hardening followed by a continuous softening stage characterized these strains. Lastly, between 8.5×10^{-3} and 1.25×10^{-2}, an important initial cyclic hardening followed by a pronounced softening stage, which turned into a nearly saturation stage near the end of the fatigue life.

Table 5
Testing conditions and corresponding saturation or half-life stress and strain values for specimens shown in Fig. 9. UA: unaged: A25 and A200: aged at 475 °C for 25 and 200 h, respectively [36].

Specimens	Applied, ε_t	Saturation or half-life σ_a (MPa)	Saturation or half-life, ε_{pl}
UA-2	2.0×10^{-3}	336	1.1×10^{-4}
UA-4	3.0×10^{-3}	450	3.0×10^{-4}
A25-1	3.0×10^{-3}	464	2.8×10^{-4}
UA-7	4.0×10^{-3}	525	1.1×10^{-3}
A200-1	4.5×10^{-3}	665	5.0×10^{-4}
A25-3	6.0×10^{-3}	656	1.3×10^{-3}
A200-3	6.5×10^{-3}	790	1.2×10^{-3}

Llanes et al. [36] studied the hardening softening response of an AISI 329 grade of DSS in the annealed ($\Delta\varepsilon/2$ values 2.0×10^{-3}, 3.0×10^{-3}, 4.0×10^{-3}) and two aged conditions mentioned in Table 5. One set of specimen was aged at 475 °C for 25 h ($\Delta\varepsilon/2$ values 3.0×10^{-3}, 6.0×10^{-3}) and another set of specimen were aged 475 °C for 200 h ($\Delta\varepsilon/2$ values 4.5×10^{-3}, 6.0×10^{-3}). They observed hardening in the first few cycles as shown in Fig. 9b. At low and intermediate $\Delta\varepsilon_{pl}/2$, such hardening was followed by either slight and rapid (low $\Delta\varepsilon_{pl}/2$) or gradual (intermediate $\Delta\varepsilon_{pl}/2$) softening. At both $\Delta\varepsilon_{pl}/2$ values a steady state of saturation was finally attained. At large $\Delta\varepsilon_{pl}/2$ annealed and aged specimens experienced a continuous softening, after hardening, till fracture. This softening behaviour was much more pronounced in the aged materials than in the annealed steel. For the largest amplitudes applied,

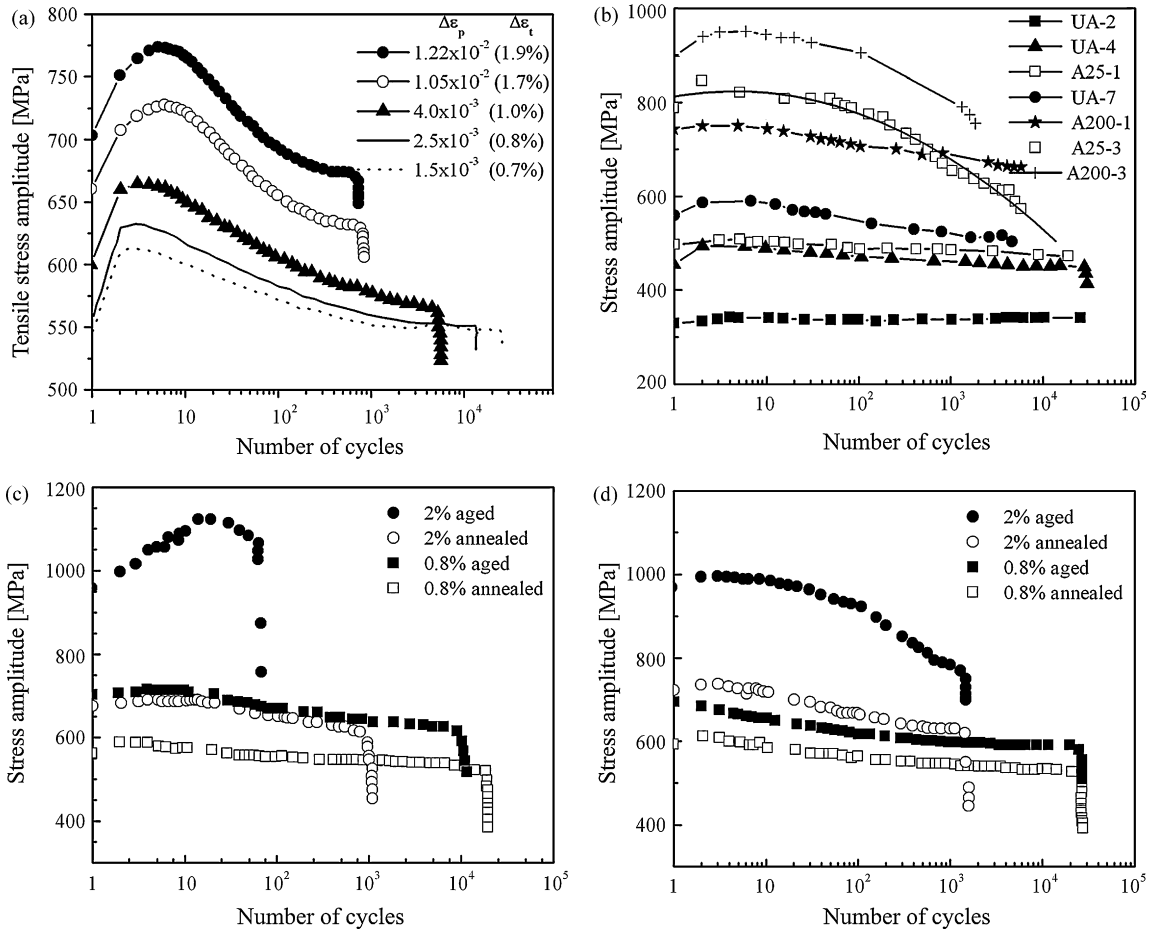

Fig. 9. Cyclic hardening/softening curves for DSS grades (a) SAF 2507 at different plastic strain ranges [70]; (b) (f) AISI 329 unaged (UA) and aged (A25, A200) condition [36]; (c) UR52N+ in the annealed and aged condition [42]; (d) BöA920 in the annealed and aged condition [42]. Fig. 9a–d is reprinted with kind permission from Elsevier.

the first few cycles of each step were characterized by load drops accompanied by audible noises characteristic of twinning. Similar hardening–softening responses were found in aged materials at large values of $\Delta\varepsilon_{pl}/2$ in spinodally decomposed high chromium ferritic stainless steels subjected to LCF [33].

Vogt et al. [42] conducted strain controlled fatigue testing of two grades of DSS designated UR52N+ and BöA920 having nitrogen content 0.24 and 0.4 wt.%, respectively, with $\Delta\varepsilon/2$ values of 4.0×10^{-3} and 1.0×10^{-2} in the annealed and aged conditions (aged at 475 °C for 200 h). The deformation curves for both alloys are shown in Fig. 9c and d. The aging treatment at 475 °C treatment did not affect the fatigue resistance, which even improved at low strain amplitude for these alloys. The aging treatment resulted in a strong increase of the stress levels for both alloys at low and high strain amplitudes. At $\Delta\varepsilon/2 = 4.0\times10^{-3}$ the curves shifted to 100 MPa higher (UR52N+) and 70 MPa higher (BöA920) but their qualitative aspect remained similar to that usually reported for as quenched DSS (slight hardening followed by a softening and a stabilization of the stress amplitude). However, the fatigue behaviour of the aged materials significantly differed from that of the annealed ones for the tests conducted at $\Delta\varepsilon/2 = 1.0\times10^{-2}$, i.e. where the plastic strain was high. In the case of the aged UR52N+ steel, the initial hardening was very pronounced. This hardening period was accompanied by a typical noise caused by twinning. On the contrary, the BöA920 steel did not exhibit such a pronounced hardening and the cyclic deformation occurred without any characteristic twinning noise. However, this material exhibits a stronger softening at high strain amplitude ($\delta_s = 0.199$ in the aged condition instead of 0.148 in the annealed condition) during about $N = 0.7N_f$ of the fatigue life.

Kwon et al. [3] observed significant degradation in the initial stage of the fatigue experiment, especially, at the large strain amplitude for the material aged at 475 °C. They did not observe significant variations in cyclic hardening/softening response with the progress of the fatigue except within the vicinity of failure.

Goh and Yip [71] conducted plastic strain controlled fatigue test ($\Delta\varepsilon_{pl}/2 = 2\times10^{-4}$ to 8×10^{-2}) with SAF 2507 grade of DSS. They observed a common trend of cyclic hardening/softening for all the imposed values of $\Delta\varepsilon_{pl}/2$. The initial rapid cyclic hardening in the case of the material investigated by them was followed by cyclic softening and final cyclic saturation. They also plotted the same curve with stress normalized by yield strength of the material to get a clear portray of the effect of plastic strain amplitude on cyclic softening and observed notable amount of cyclic softening only when σ/σ_{ys} ratio was above 0.8.

3.3.2. Cyclic stress-strain curve

The CSSC plotted by Magnin and Lardon for DSS consist of two separate stages. The transition point was identified at $\Delta\varepsilon_{pl}/2 = 1.0\times10^{-3}$ [34]. The curve changes from one of a high strain-hardening rate in the first regime, to a low strain-hardening rate in the second regime. Llanes et al. [36] have described the cyclic stress–strain response of DSS in the annealed and aged conditions in three stages in terms of plastic strain amplitudes ($\Delta\varepsilon_{pl}/2 < 10^{-4}$, $10^{-4} < \Delta\varepsilon_{pl}/2 < 10^{-3}$, $\Delta\varepsilon_{pl}/2 > 10^{-3}$) each amenable to be characterized by well-defined and distinct cyclic deformation mechanisms. Goh and Yip [71] identified two separate regimes with different strain-hardening rates in the CSSC plotted by them. The first regime, at $\Delta\varepsilon_{pl}/2 < 7.0\times10^{-3}$, had a high cyclic strain-hardening rate, while the second regime, at $\Delta\varepsilon_{pl}/2 > 7.0\times10^{-3}$, had a strain-hardening rate that is less pronounced than the first.

3.3.3. Cyclic life

Magnin and Lardon [34] detected the change of slope of the Coffin-Manson curves of DSS at $\Delta\varepsilon_{pl}/2$ value of 1.0×10^{-3}. Mateo et al. [72] conducted experiments in an extended range of plastic strain amplitude ($2.9\times10^{-5} < \Delta\varepsilon_{pl}/2 < 6.6\times10^{-3}$) and the Coffin-Manson curve in their case is subdivided into three regimes: stage I $\Delta\varepsilon_{pl}/2 < 1.0\times10^{-4}$ with austenite like behaviour; stage II, $<1.0\times10^{-4} < \Delta\varepsilon_{pl}/2 < 6.0\times10^{-4}$ with mixed austenite–ferrite like response; stage III, $\Delta\varepsilon_{pl}/2 > 6.0\times10^{-4}$ with pure ferrite like behaviour. But the above works were reported for DSS grades containing 0.07 wt.% nitrogen. And the multiple factors that can affect the fatigue life can be realized from the studies conducted by Akdut [65]. He studied the phase morphology and fatigue life of nitrogen alloyed duplex stainless steels and observed the fatigue lives of DSS were influenced by numerous parameters such as processing history and chemical composition and, thus by morphological anisotropy, morphological scale and nitrogen content. He showed that change in increasing morphological anisotropy and decreasing morphological scale has an increasing effect on the fatigue life of DSS. Contrary to single-phase austenitic stainless steel, increasing the nitrogen content in DSS did not appear to increase the fatigue life. However, nitrogen in combination with the morphological scale and anisotropy apparently alters the extent of each of the three regime proposed by Mateo et al. [72]. Akdut also postulated the dependence of fatigue life on crystallographic texture.

Kwon et al. [3] also obtained such linearized plots in their investigation on CF8M cast grade of DSS. The Coffin-Manson curve is plotted but not discussed by Vogt et al. [42]. However, from their plot it appears that the fatigue life is decreased as a result of aging treatment for the range of strain amplitude investigated by them for the alloy with low nitrogen content. The fatigue life in the aged conditions appear to be approaching the fatigue life in the annealed condition as the strain amplitude was decreased. Whereas, aging treatment at 475 °C seems to have no or very little effect on the fatigue life of alloy with high nitrogen content.

3.3.4. Substructural evolution

Considering the transition in the CSSC curve towards a rapid cyclic softening in the aged condition with increase in plastic strain amplitude and the fatigue life curves attempts have been made to look into the substructural evolution in the embrittled condition. The uniaxial structures such as bundles, channel-vein and loop patches are known to form at the beginning of cycling and the initial hardening has been attributed to the formation of these structures [73]. The formation of PSB is an indication of cyclic softening as they can accommodate more plastic strain compared to the channel-vein structure [74]. So observation of these bundles is a common feature. Llanes et al. [36] observed a dominant structure evolution in the ferritic grain of AISI 329 grade of DSS at $\Delta\varepsilon_{pl}/2 > 1.0\times10^{-3}$ with the development of vein into wall structure. Kruml et al. [75] observed two characteristic types of dislocation structure in the ferritic phase of DIN X2CrNiMoN22-5 grade of DSS at $\Delta\varepsilon_{pl}/2 = 4.5\times10^{-3}$. They observed vein and wall structure and a few short walls perpendicular to the direction of primary walls. They indicate that to be the onset of biaxial structure formation. Alvarez-Armas et al. [66] observed bundles of dislocation in the ferritic phase at $\Delta\varepsilon/2 = 4.0\times10^{-3}$ in the bulk of the sample. But interestingly they observed different features like homogeneous unidirectional wall aligned in the trace of (1 1 0) plane in a specimen sliced near the surface. These wall structures was spread over both ferritic and austenitic grains and was found to compliance with *K–S* orientation relationship. This observation is an indication that a direct relationship cannot be established between the slip markings on the surface, which are the plane traces and the dislocation substructure in the bulk of the specimen. Mateo et al. [72] observed cell, wall structure and loop patches corresponding to half-life $\Delta\varepsilon_{pl}/2 = 6.0\times10^{-3}$. The structures observed in the ferritic phase of DSS in the similar values of strain amplitudes are given in Table 6.

The substructural evolution in the austenitic phase is well documented [75,76]. The dislocation planar arrays are usually observed

Table 6
The strain localization features observed in the ferritic phase of 475 °C embrittled DSS.

Name of researchers	DSS grade	Strain amplitude	Dislocation substructure
Sahu [56]	DIN W Nr. 1.4460	$\Delta\varepsilon/2 = 8.0 \times 10^{-3}$	Coalescence of the array of and disappearance of the needle-shaped precipitate
Alvarez-Armas et al. [66]	Low nitrogen DIN W Nr. 1.4460	$\Delta\varepsilon/2 = 4.0 \times 10^{-3}$	Bundles of dislocation
Mateo et al. [72]	SAF 2507	$\Delta\varepsilon_{pl}/2 = 6.0 \times 10^{-3}$	Cell structure, developed wall structure, dense loop patches and poorly defined channels
Kruml et al. [75]	DIN X2CrNiMoN22-5	$\Delta\varepsilon_{pl}/2 = 4.5 \times 10^{-3}$	Veins, wall structure and a few perpendicular walls indicating the onset of formation of biaxial labyrinth structure

at low strain amplitude. Two major factors those influence the dislocation behaviour are, (a) stress (b) nitrogen content [76]. At higher values of strain amplitudes the secondary slip system is activated and cross slip can initiate and as a result cell structure are observed. Apart from higher stress nitrogen is also known to modify the substructural evolution in austenite. With increase in nitrogen content the SFE value decreases. It means nitrogen promote planar slip increasing the fatigue strength and inhibiting strain localization.

The cyclic softening of the ferritic phase aged at 475 °C was initially investigated in pure ferritic alloys [33]. Park et al. [33] attributed the observed low cycle fatigue softening for their iron–26chromium–1molybdenum alloy to the localized demodulation of the spinodal microstructure due to irreversibly dislocation motion. The same mechanism has also been observed in fcc alloys those undergo spinodal decomposition [77,78]. Anglada et al. [79] have reported a similar softening behaviour during cyclic deformation of an aged iron–28chromium–4nickel–niobium alloy and attributed this to the demodulation of spinodal microstructure. They considered the slip symmetry of bcc alloys and a more pronounced asymmetry at higher values of plastic strain amplitude as being responsible for such kind of demodulation.

In explaining the involvement of the ferritic phase of the aged material in plastic deformation at higher values of plastic strain amplitude, Llanes et al. [36] postulated that the ferritic phase carry out plastic deformation through gradual demodulation of the spinodal microstructure by dislocation glide irreversibility and deformation twinning. However, they observed this behaviour heterogeneously and attributed this to grain orientation and cyclic behaviour of neighbouring grains.

Sahu [56] attributed the cyclic softening of the ferritic phase in DSS grade DIN W Nr. 1.4462 at higher plastic strain amplitude to the coalescence of the array of precipitates observed in Fig. 5 along with disappearance of the needle-shaped precipitate. The TEM image of the LCF tested sample is shown in Fig. 10.

3.3.5. *Fatigue crack initiation in DSS embrittled at 475 °C*

Evolution of surface roughness, subsequent nucleation and growth of short crack in DSS by cyclic loading is strongly influenced by the microstructural parameters, i.e. grain size, grain orientation, grain and phase boundary geometry or the new phase called grain boundary character distribution (GBCD) and precipitates. The crack initiation and growth in particular grain in DSS depend on the orientation, inherent strength and toughness properties of neighbouring grains and it is very important to know and understand how these factors determines fatigue damage evolution. Taisne et al. [80] in a recent study on the role of interfaces in fatigue deformation mechanism in DSS bicrystal observed that interphase interface geometry and elasticity affects the dislocation transmission process. Düber [69] in a recent investigation on the same grade of DSS showed that crack propagation in the short crack regime can be subdivided into two basic mechanisms: operating either by single-slip (crystallographic propagation) and double-slip (propagation perpendicular to loading axis), giving rise to substantially different propagation rates. Additionally, it was found that a crack, which has grown in double-slip, can change to the single-slip mechanism again, when entering a new grain and no adequate second slip plane is available. They also determined that the $\alpha\gamma$ phase boundary offers more resistance to slip transfer as compared to $\alpha\alpha$ and $\gamma\gamma$ grain boundaries. Alvarez-Armas et al. [66] observed that the efficiency of the coupling between phases seems to play an important role in the crack formation process. Stolarz and Foct [41] on their study on specific features of two phase alloys response to cyclic deformation observed that the short crack initiation sites (brittle or ductile phase, interfaces), the cyclic damage mode (single or multiple cracking) and consequently the fatigue life, depend both on morphological and topological parameters of the microstructure and on the difference on the mechanical properties of constitutive phases. These studies justify the increasing interest in the study of the influence of microstructural parameters on the evolution of surface fatigue damage and the subsequent crack nucleation.

In DSS aged at 475 °C, the difference between the mechanical properties of austenite and ferrite become more pronounced. In the case of cyclic loading of DSS in annealed condition, slip bands represent the main crack initiation site either in austenite or ferrite depending on the applied strain amplitude. However, the slip incompatibilities created at the interphase boundaries after the aging treatment at 475 °C may lead to a non-uniform distribution of surface damage. In a recent investigation, in situ tensile tests have been performed on a thermally aged DSS and EBSD technique has been used to correlate local phase morphology with crystallographic properties [22]. Sahu [56] conducted completely reversed ($R = -1$) interrupted stress-controlled fatigue test at $\Delta\sigma/2 = 400$ and 500 MPa to identify the crack initiation sites and relate these to the crystallographic parameters obtained from EBSD-OIM scans and observed that the crack initiation sites are the slip markings corresponding to $\{1\,1\,1\}$ plane traces in the austenitic grains at $\Delta\sigma/2 = 400$ MPa and $\Sigma 3$ CSL boundary in the austenitic grain at $\Delta\sigma/2 = 500$ MPa as shown in Fig. 11.

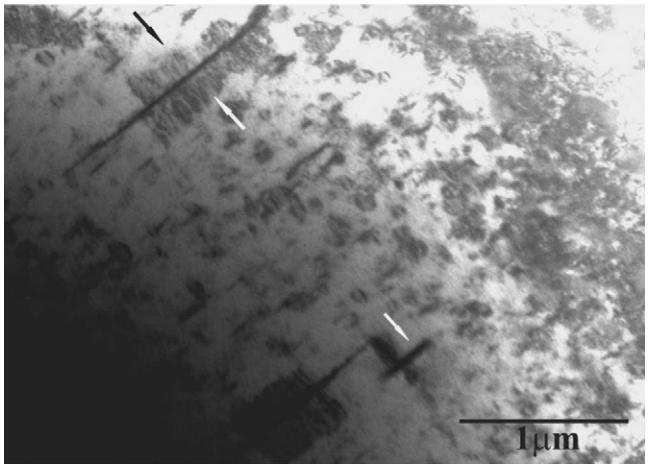

Fig. 10. TEM bright field image of the ferritic phase in DSS grade DIN W Nr. 1.4462 in the embrittled condition. The arrowed regions are the highly strained zones, the precipitates show coffee bean contrast at the center; $\Delta\varepsilon_{pl}/2 = 3.7 \times 10^{-3}$ [56].

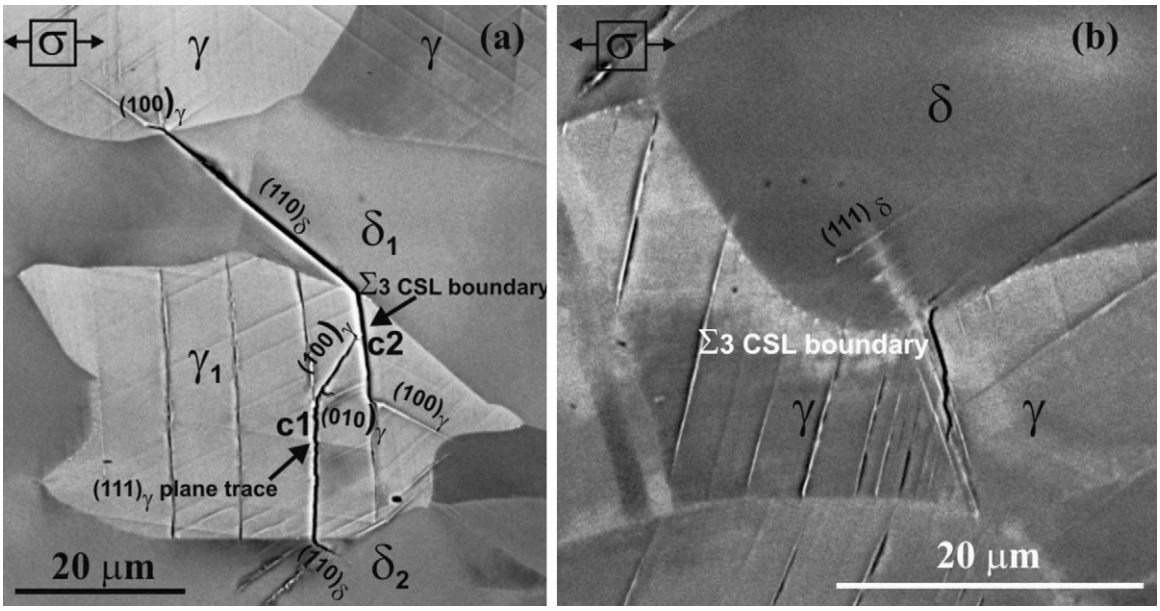

Fig. 11. Fatigue crack initiation in a DSS grade DIN W Nr. 1.4462 aged at 475 °C for 100 h. (a) The growth of crack c2 observed after $N = 27{,}000$ cycles at $\Delta\sigma/2 = 400$ MPa; (b) crack initiation at Σ3 CSL boundary at $\Delta\sigma/2 = 500$ MPa [56].

3.3.6. High cycle fatigue behaviour

Nyström and Karlsson [37] suggested that a careful balance of the ferrite content in a duplex microstructure can eliminate the effect of embrittlement to a certain extent, retaining the advantage of duplex microstructure. They showed that with an alloy containing 25% ferrite and 75% austenite, the high cycle fatigue properties are little affected by aging at 475 °C for 100 h. The nominal fatigue crack growth rates, da/dN, as a function of the stress intensity range, ΔK, are shown in Fig. 12. As can be seen, the annealing at 475 °C of the duplex material has only a minor influence on the crack growth properties with a slight shift to the left of crack growth curve for the embrittled condition. This means that the crack growth resistance is essentially insensitive to the hardening caused by the heat treatment.

Llanes et al. [38] in their work on high cycle fatigue behaviour of aged DSS showed that the large increase in the overall monotonic strength is not completely reflected in its fatigue strength. They tested one set of samples in the unaged condition (UA) and another after aging treatment at 475 °C for 200 h (A200) S–N plot is shown in Fig. 13. They observed that the high cycle fatigue strength is strongly affected by the crack nucleation stage in the softer phase The fatigue strength improvement results from the higher cyclic yield stress of the spinodally-hardened ferrite which induces an increasing difficulty for early propagation of microcracks nucleated within austenite into and through the ferritic matrix.

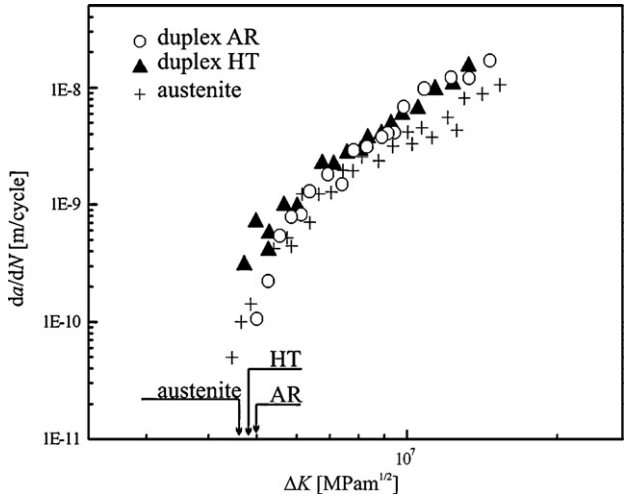

Fig. 12. da/dN–ΔK relationship for DSS and austenitic grade stainless steel. Reprinted with kind permission from Elsevier from [37].

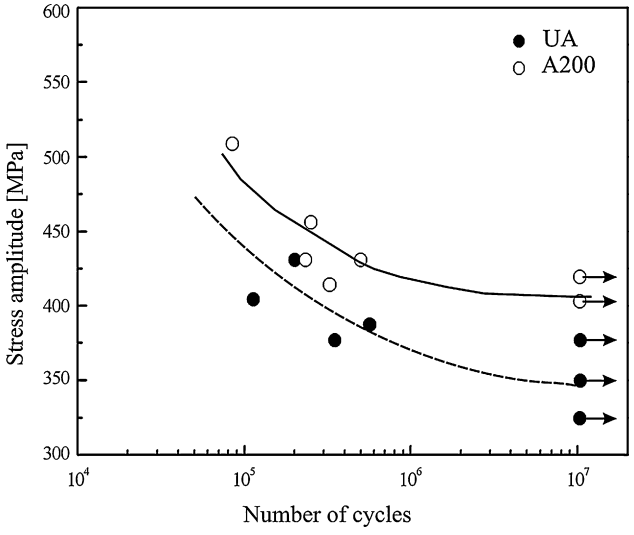

Fig. 13. HCF behaviour for unaged (UA) and aged (A200) DSS grade AISI 329. Reprinted with kind permission from Elsevier from [38].

4. Conclusions

The precipitation of α′ in the ferritic phase during 475 °C embrittlement is a well-known phenomenon. There are a large number of studies reported in the literature on this embrittlement behaviour in the iron–chromium binary alloy system. The ferritic phase in the DSS also embrittles with a similar mechanism. However, from the review it is apparent that the alloying elements play a significant role in altering the thermodynamics and kinetics of precipitations. DSS is highly alloyed compared to the binary iron–chromium material and there is an increasing trend to further alloy it to obtain

improved mechanical properties and corrosion resistance. Studies reported on the effect of these individual alloying elements on 475 °C embrittlement of DSS is very scarce and is a subject of further research.

It is observed that the ferrite content in a duplex microstructure varies from about 10% in the as cast grades of DSS to about 50% in the wrought DSS grades. Depending on the requirement the ferrite content in DSS is tailored to give the best combination of strength and corrosion resistance. However, the trend is to increase the ferrite content to increase the strength properties and reduce the material requirement to bring down the cost. As it is seen the morphology and spacing of ferrite in the microstructure plays a significant role in determining the crack growth resistance of DSS. This also is a very interesting area for further research.

A substantial number of investigations are also reported on the estimation of residual mechanical properties of DSS as a result of precipitation of α' during 475 °C embrittlement. From the review of all the work it is seen that attempts are made to determine the end-of-life mechanical properties either through experimental techniques with miniaturized specimens or standard specimens with accelerated aging or indirect estimations from empirical formulations relating mechanical properties to chemical composition. However, these are all approximate techniques. The nature of α' precipitation during 475 °C of DSS does not result in appreciable change, in the determinable microstructural parameters such as grain size distribution, precipitate size, etc. As a result number of studies reported in the area of microstructure–property relationship are very limited. However, aging results in the rearrangement of dislocations in the ferritic phase. This rearrangement of dislocation due to the precipitation of α' significantly influences the deformation behaviour. Efforts have been made by some researchers to look into the substructural evolution in the ferritic and austenitic phases during 475 °C embrittlement. Number of investigations in this area is extremely scarce. The gray area remains in the change in deformation mechanisms due to 475 °C embrittlement of DSS in the ferritic and austenitic phase. These studies may open up new horizons for the alloy developments in order to overcome the problem of 475 °C embrittlement.

Acknowledgement

The financial support by Deutscher Akademischer Austausch Dienst (DAAD) at the beginning of the work on "475 °C embrittlement of duplex stainless steel" by Mr. J.K. Sahu at IFWT Siegen, is gratefully acknowledged.

References

[1] S. Kawaguchi, N. Sakamoto, G. Takano, F. Matsuda, Y. Kikuchi, L. Mráz, Nuclear Engineering and Design 174 (3) (1997) 273–285.
[2] J.S. Cheon, I.S. Kim, Journal of Nuclear Materials 278 (1) (2000) 96–103.
[3] J. Kwon, S. Woo, Y. Lee, J. Park, Y. Park, Nuclear Engineering and Design 206 (1) (2001) 35–44.
[4] V. Calonne, C. Berdin, B. Saint-Germain, S. Jayet-Gendrot, Journal of Nuclear Materials 327 (2–3) (2004) 202–210.
[5] N. Giel, Proceedings of 5th World Conference, Duplex Stainless Steel, 1997.
[6] A. El-Batahgy, B. Zaghloul, Materials Characterization 54 (2005) 246–253.
[7] L. Smith, Proceedings of Duplex America Conference, 2000.
[8] J. Olsson, Acom, 1-2-86 (1986) 18–23.
[9] J. Nordstrom, Acom, 3-94 (1994) 1–6.
[10] A. Tuomi, Proceedings of Duplex America Conference, 2000.
[11] J. Charles, B. Vincent, Proceedings of 5th World Conference, Duplex Stainless Steel, 1997.
[12] B. Heuer, Proceedings of Duplex America Conference, 2000.
[13] H.D. Solomon, L.M. Levinson, Acta Metallurgica 26 (3) (1978) 429–442.
[14] D. Chandra, L.H. Schwartz, Metallurgical Transactions 2 (1971) 511–519.
[15] P.J. Grobner, Metallurgical Transactions 4 (1973) 251–260.
[16] J. Johansson, M. Odén, Metallurgical and Materials Transactions A 31 (2000) 1557–1570.
[17] R.N. Gunn, Duplex Stainless Steels: Microstructure, Properties and Applications, Woodhead Publishing, 1997.
[18] F.J. Ager, S. Elmrabet, A. Paúl, A. Cea-Naharro, M.D. Ynsa, M.A. Respaldiza, J.A. Odriozola, Nuclear Instruments and Methods in Physics Research Section B: Beam Interactions with Materials and Atoms 188 (1–4) (2002) 96–101.
[19] W. Zielinski, W. Witnicki, M. Barstch, U. Messerschmidt, Material Chemistry and Physics 81 (2–3) (2003) 476–479.
[20] S. Bugat, J. Besson, A.-F. Gourgues, F. N'Guyen, A. Pineau, Materials Science and Engineering A 317 (2001) 32–36.
[21] O.A. Hilders, M. Ramo, N.D. Peña, L. Sáenz, Journal of Materials Engineering and Performance 8 (1) (1999) 87–90.
[22] A. Gironès, L. Llanes, M. Anglada, A. Mateo, Materials Science and Engineering A 367 (1–2) (2004) 322–328.
[23] M.K. Miller, K.F. Russell, Applied Surface Science 94–95 (1996) 398–402.
[24] L. Devillers-Guerville, J. Besson, A. Pineau, Nuclear Engineering and Design 168 (1–3) (1997) 211–225.
[25] T.J. Marrow, N. Bury, Fatigue and Fracture of Engineering Materials and Structures 20 (4) (1997) 565–571.
[26] S.G. Druce, G. Gage, E. Popkiss, International Journal of Pressure Vessels and Piping 33 (1) (1988) 59–81.
[27] Y. Tujikura, S. Urata, Nuclear Engineering and Design 191 (2) (1999) 255–261.
[28] S. Jayet-Gendrot, P. Ould, T. Meylogan, Nuclear Engineering and Design 184 (1) (1998) 3–11.
[29] P. Le Delliou, P. Julisch, K. Hippelein, G. Bezdikian, Nuclear Engineering and Design 193 (3) (1999) 273–282.
[30] M.D. Mathew, L.M. Lietzan, K.L. Murty, V.N. Shah, Materials Science and Engineering A 269 (1–2) (1999) 186–196.
[31] O.K. Chopra, H.M. Chung, Nuclear Engineering and Design 89 (2–3) (1985) 306–318.
[32] Assessment and management of ageing of major nuclear power plant components important to safety; Primary piping in PWRs, Technical Report of InternationalAtomic Energy Agency, IAEA-TECDOC-1361, July 2003.
[33] K.-H. Park, J.C. Lasalle, L.H. Schwartz, Acta Metallurgica 33 (2) (1985) 205–211.
[34] T. Magnin, J.M. Lardon, Materials Science and Engineering 104 (1988) 21–28.
[35] T.J. Marrow, J.E. King, Materials Science and Engineering A 183 (1–2) (1994) 91–101.
[36] L. Llanes, A. Mateo, L. Iturgoyen, M. Anglada, Acta Materialia 44 (10) (1996) 3967–3978.
[37] M. Nyström, B. Karlsson, Material Science and Engineering A 215 (1–2) (1996) 26–38.
[38] L. Llanes, A. Mateo, P. Violan, J. Méndez, M. Anglada, Materials Science and Engineering A 234–236 (1997) 850–852.
[39] T.H. Kang, D.M. Li, Y.D. Lee, C.S. Lee, Materials Science and Engineering A 251 (1–2) (1998) 192–199.
[40] F. Iacoviello, M. Boniardi, G.M. La Vecchia, International Journal of Fatigue 21 (1999) 957–963.
[41] J. Stolarz, J. Foct, Materials Science and Engineering A 319–321 (2001) 501–505.
[42] J.-B. Vogt, K. Massol, J. Foct, International Journal of Fatigue 24 (6) (2002) 627–633.
[43] S. Jayet-Gendrot, P. Gilles, C. Migné, Nuclear Engineering and Design 197 (1–2) (2000) 141–153.
[44] M.K. Miller, P.A. Beaven, R.J. Lewis, G.D.W. Smith, Surface Science 70 (1) (1978) 470–484.
[45] J.E. Brown, G.D.W. Smith, Surface Science 246 (1–3) (1991) 285–291.
[46] H.M. Chung, International Journal of Pressure Vessels and Piping 50 (1–3) (1992) 179–213.
[47] F. Danoix, B. Deconihout, A. Bostel, P. Auger, Surface Science 266 (1–3) (1992) 409–415.
[48] K.L. Weng, H.R. Chen, J.R. Yang, Materials Science and Engineering A 379 (1–2) (2004) 119–132.
[49] J.S. Park, Y.K. Yoon, Scripta Metallurgica et Materialia 32 (8) (1995) 1163–1168.
[50] G. Reidrich, F. Loib, Archiv für das Eisenhüttenwesen 15 (1941) 175–182.
[51] J.M. Blackburn, J.J. Nutting, Iron and Steel Institute 202 (1964) 610–613.
[52] M.B. Cortie, H. Pollak, Materials Science and Engineering A 199 (1995) 153–163.
[53] Assessment and management of ageing of major nuclear power plant components important to safety; PWR vessel internals. Technical Report of International Atomic Energy Agency, IAEA-TECDOC, 1119, July 2003.
[54] A.B. Johnson Jr, S.K. Sundaram, F.A. Garner, Program plan for acquiring and examining naturally aged materials and components from nuclear reactors. Pacific Northwest National Laboratory, Richland, WA, PNNL-13930, December 2001.
[55] S. Bonnet, J. Bourgoin, J. Champredonde, D. Guttmann, M. Guttmann, Materials Science and Technology 6 (1990) 221–229.
[56] J.K. Sahu, Dissertation, University of Siegen, Germany, 2008.
[57] R.M. Fisher, E.J. Dulis, K.G. Carrol, Transactions AIME 197 (1953) 690–695.
[58] R.O. Williams, Trans. TMS-AIME 212 (1958) 497–502.
[59] E.Z. Vintaikin, A.A. Loshmanov, Physics of Metals and Metallography 22 (1966) 473–476.
[60] J.W. Cahn, Acta Metallurgica 9 (1961) 795–801.
[61] J.E. Hilliard, in: H.I. Aaronson (Ed.), Phase Transformations, American Society for Metals, Metals Park, Ohio, 1970.
[62] M.K. Miller, J. Bentley, Materials Science and Technology 6 (1990) 285–292.
[63] A. Mateo, L. Llanes, M. Anglada, A. Redjaimia, G. Metauer, Journal of Materials Science 32 (1997) 4533–4540.
[64] T. Bliznuk, M. Mola, E. Polshin, M. Pohl, V. Gavriljuk, Materials Science and Engineering A 405 (2005) 11–17.
[65] N. Akdut, International Journal of Fatigue 21 (1999) 97–103.

[66] I. Alvarez-Armas, M.C. Marinelli, J.A. Malarria, S. Degallaix, A.F. Armas, International Journal of Fatigue 29 (2007) 758–764.
[67] T. Takemoto, K. Mukai, K. Hoshini, Transactions ISIJ 26 (1986) 337–344.
[68] A. Girones, P. Villechaise, A. Mateo, M. Anglada, J. Mendez, Material Science and EngineeringA 387–389 (2004) 516–521.
[69] O. Düber, Untersuchungen zum Ausbreitungsverhalten mikrostrukturell kurzer Ermüdungsrisse in zweiphasigen metallischen Werkstoffen am Beispiel eines austenitissch-ferritischen Duplexstahls. Ph.D. Dissertation, Universität Siegen, Germany, 2007.
[70] I. Alvarez-Armas, M.C. Marinelli, S. Herenu, S. Degallaix, A.F. Armas, Acta Materialia 54 (2006) 5041–5049.
[71] C.S. Goh, T.H. Yip, Metallurgical and Materials Transactions A 33A (2002) 3433–3442.
[72] A. Mateo, A. Gironès, J. Keichel, L. Llanes, N. Akdut, M. Anglada, Materials Science and Engineering A 314 (1–2) (2001) 176–185.
[73] R.J. Amodeo, N.M. Ghoniem, Physical Review B 41 (10) (1990) 6968–6976.
[74] U. Essmann, H. Mughrabi, Philosophical Magazine A 40 (6) (1979) 731–756.
[75] T. Kruml, J. Polak, K. Obrtlik, S. Degallaix, Acta Materialia 45 (12) (1997) 5145–5151.
[76] I. Karaman, H. Sehitoglu, Y.I. Chumlyakov, H.J. Maier, JOM 54 (7) (2002) 31–37.
[77] H.-R. Sinning, Acta Metallurgica 30 (1982) 1019–1026.
[78] R.K. Ham, J.S. Kirkald, J.T. Plewes, Acta Metallurgica 15 (1967) 861–869.
[79] M. Anglada, J. Rodríguez, A. Isalgué, Scripta Metallurgica 23 (9) (1989) 1633–1638.
[80] A. Taisne, B. Decamps, L. Priester, Composite Interfaces 13 (1) (2006) 89–102.